Light storage in an optically thick atomic ensemble under conditions of electromagnetically induced transparency and four-wave mixing

Nathaniel B. Phillips,[1] Alexey V. Gorshkov,[2] and Irina Novikova[1]

[1]*Department of Physics, College of William and Mary, Williamsburg, Virginia 23185, USA*
[2]*Institute for Quantum Information, California Institute of Technology, Pasadena, California 91125, USA*

We study the modification of a traditional electromagnetically induced transparency (EIT) stored-light technique that includes both EIT and four-wave mixing (FWM) in an ensemble of hot Rb atoms. The standard treatment of light storage involves the coherent and reversible mapping of one photonic mode onto a collective spin coherence. It has been shown that unwanted, competing processes such as four-wave mixing are enhanced by EIT and can significantly modify the signal optical pulse propagation. We present theoretical and experimental evidence to indicate that, while a Stokes field is indeed detected upon retrieval of the signal field, any information originally encoded in a seeded Stokes field is not independently preserved during the storage process. We present a simple model that describes the propagation dynamics of the fields and the impact of FWM on the spin wave.

I. INTRODUCTION

The successful development of practical quantum information applications relies to a large extent on the availability of high-efficiency and high-fidelity memory for quantum states of photons. Recently, several promising realizations of such a quantum memory were demonstrated, which are based on the reversible mapping of photon quantum states onto long-lived collective coherences in ensembles of atoms [1–5]. In the majority of these protocols, an atomic ensemble of sufficiently high optical depth is necessary in order to achieve high memory efficiency. However, in this case, some unwanted competing processes may interfere with quantum memory performance, reducing its efficiency and fidelity [6–12].

In this paper, we investigate the propagation and storage of weak optical signal pulses in an optically thick vapor based on electromagnetically induced transparency (EIT) [1,13]. Traditionally, an EIT-based light storage scheme considers the simultaneous interaction of a strong control field and a weak signal field in a Λ-type configuration, in which two ground-state hyperfine levels are linked with a common excited state, as shown in Fig. 1(a). In this case, the control field strongly couples the propagation of the signal optical field with a collective long-lived ground-state atomic spin coherence (spin wave) [1,14], resulting in a reduced group velocity for signal pulses ("slow light"). Adiabatic turn-off of the control field maps the quantum state of the signal field onto the spin wave, which can be stored and later retrieved by restoring the control field intensity.

Such an EIT quantum memory has been realized for both weak classical and nonclassical signal pulses (for recent reviews, see Refs. [3–5]). Some recent publications [15–17] investigated the optimal performance of such an EIT memory and have confirmed that high optical depth is necessary to improved storage efficiency. For example, 90% memory efficiency requires an optical depth $\alpha_0 L > 100$ [18]. On the other hand, an optically dense coherent atomic medium is also known to enhance competing undesired effects, such as resonant four-wave mixing (FWM) in a double-Λ

configuration. In this FWM process, the far-detuned interaction of the control field, which resonantly drives the $|s\rangle$-$|e\rangle$ transition [see Fig. 1(a)], with atomic ground-state coherence enhances the generation of an off-resonant Stokes optical field [α' in Fig. 1(a)]. In turn, the presence of a Stokes field strongly affects signal pulse propagation, and the propagation of both signal and Stokes fields become a result of the interference between regular EIT and FWM processes [11,12,19].

Under such conditions, the simplified treatment of an EIT-based quantum memory in a single-Λ system is incomplete and fails to describe light storage at high optical depths [17]. In this work, we explore the mechanisms governing propagation of signal and Stokes pulses under EIT-FWM conditions and develop an intuitive analytical treatment of this problem. In particular, we investigate the prospect of their light storage; that is, a process in which both signal and Stokes pulses are reversibly mapped onto a long-lived spin coherence and thus can be faithfully recreated after some storage period. Recent experiments [20] have shown that a spontaneously generated Stokes field can be detected upon retrieval of a signal field from a spin coherence. Based on these results, one might anticipate that the spin wave might function, at least to some extent, as a memory for both pulses. In our experiments, both input signal and Stokes fields have nonzero amplitudes before entering the atomic medium. We observed that, under certain experimental conditions, both signal and Stokes pulses appear to be delayed due to the interaction with atoms; that is, both signal and Stokes outputs are nonzero even after the input signal and Stokes fields are turned off. Moreover, when the control field is turned off for some time and then later turned on, output pulses are retrieved in both channels, as shown in Fig. 1(b). However, careful experimental and theoretical investigation shows that this is not a two-mode storage; that is, the signal and Stokes fields cannot be stored independently. Instead, under EIT-FWM conditions, the collective ground-state spin coherence is determined by a particular combination of signal and Stokes fields. Moreover, both retrieved fields are, in fact, only very weakly sensitive to the input Stokes field. To explain these effects, we present an intuitive analytical picture of the effects
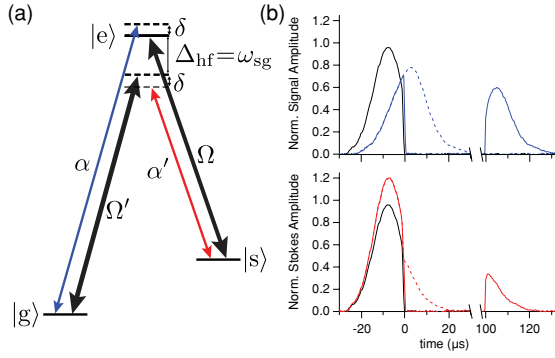
FIG. 1. (Color online) (a) The double-Λ system used in theoretical calculations. In our case, $|g\rangle$ and $|s\rangle$ correspond to the ^{87}Rb ground-state hyperfine sublevels $|F,m_F\rangle = |1,1\rangle, |2,1\rangle$, respectively; $|e\rangle$ corresponds to the excited state $|F',m_{F'}\rangle = |2,2\rangle$. Ω, Ω' represent the Rabi frequencies of the same control field acting on two different transitions, while α and α' represent the Rabi frequencies of the signal and Stokes fields, respectively. (b) Sample data for light storage for signal (top) and Stokes (bottom) pulses at a temperature $T = 70\,^\circ$C (optical depth $\alpha_0 L = 52$). Dashed lines show propagation of these pulses under the slow-light regime (constant control field). The black curve is a far-detuned reference pulse. We scaled the pulses to the maximum amplitude of the reference pulse.

of FWM on the signal and Stokes pulses and on the atomic spin coherence.

II. EXPERIMENTAL ARRANGEMENTS

A schematic of the experimental setup is shown in Fig. 2. The output from an external cavity diode laser (ECDL) locked to the Rubidium D_1 transition ($\lambda = 795$ nm) passed through a polarizing beam splitter (PBS), which split off a fraction of the beam for use as a reference frequency, while the rest of the beam was coupled into a single-mode optical fiber (SMF) to improve its transverse intensity distribution. All experimental data shown below were obtained using weak classical laser pulses. To ensure the best spatial overlap and mutual phase coherence, all three optical fields were derived from a single laser beam by phase modulation. After the fiber, the beam passed through an acousto-optical modulator (AOM), and
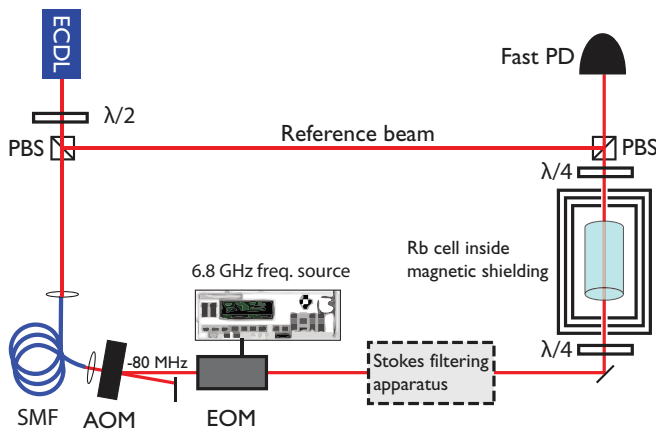

FIG. 2. (Color online) Schematic of the experimental arrangements. See text for abbreviations.

the -1 diffraction beam (downshifted by 80 MHz) then passed through an electro-optical phase modulator (EOM) operating at the frequency of the ground-state hyperfine splitting of ^{87}Rb [$\Delta_{\rm hf}/(2\pi) = 6.835$ GHz]. This phase modulation produced two first modulation sidebands at $\pm\Delta_{\rm hf}$ of nearly equal amplitudes and opposite phases. The zeroth-order (carrier frequency) field was tuned to the $5^2 S_{1/2} F = 2 \rightarrow 5^2 P_{1/2} F' = 2$ transition and acted as the control field Ω [21]. The $+1$ modulation sideband, tuned near the $5^2 S_{1/2} F = 1 \rightarrow 5^2 P_{1/2} F' = 2$ transition, played the role of the signal field, while the -1 sideband acted as the Stokes field. The resulting beam was collimated to a diameter of 1.9 mm or 2.7 mm, as specified below, and circularly polarized with a quarter-wave plate ($\lambda/4$). Typical peak control and signal field powers were approximately 14 mW and 40 μW, respectively. For some experiments, we attenuated the amplitude of the Stokes field as described in Refs. [12,17].

A cylindrical Pyrex cell, of length $L = 75$ mm and diameter 22 mm, containing isotropically enriched ^{87}Rb and 30 Torr Ne buffer gas so that the pressure-broadened optical transition linewidth was $2\gamma/(2\pi) = 290$ MHz [22], was mounted inside trilayer μ-metal magnetic shielding in order to reduce the effects of stray magnetic fields. The temperature of the cell and, correspondingly, the concentration of Rb in the vapor phase, was controlled using a bifilar resistive heater wound around the inner-most shield layer. Experimental temperatures ranged from 50 to 80 $^\circ$C, which corresponded to changes in Rb density from 1.1×10^{11} cm^{-3} to 1.2×10^{12} cm^{-3} and to a range of optical depths $\alpha_0 L$ between 10 and 110. After the cell, the light beam was linearly polarized with a $\lambda/4$ plate, recombined with the unshifted reference beam, and sent via a multimode optical fiber to a fast photodetector (PD). The beat note signals between each of the $+1$ and -1 modulation sidebands and the reference field were measured using a microwave spectrum analyzer. Because of the 80 MHz frequency shift introduced by the AOM, the different beat note frequencies of each sideband with the reference field allowed for independent measurement of their amplitudes.

Simultaneously programmed modulation strengths of the AOM and EOM allowed for independent control over the temporal envelopes of the control field and the signal or Stokes fields. In this set of measurements, we used constant levels of the control field for both writing and retrieval stages and truncated Gaussian waveforms for the signal and Stokes fields. Each slow- and stored-light measurement was preceded by a 400 μs pulse of the control field at maximum intensity to ensure optical pumping of the atoms in the interaction region into state $|g\rangle$.

Similar to Refs. [12,17], we extracted the spin-wave decoherence time τ_s by measuring the reduction of the retrieved pulse energies in both the signal and Stokes channels as a function of storage time and fitting to an exponential decay e^{-t/τ_s}. Figure 3 presents a sample measurement of the decay rate at $T = 70\,^\circ$C ($\alpha_0 L = 52$), for which we measured $\tau_s = 300\ \mu$s. To aid in comparison, we normalized the signal and Stokes retrieval energies by their respective zero-storage-time values, which in this case was $\approx$40% for signal and $\approx$5% for Stokes. Both the exponential trend and the correspondence between the data obtained with the signal and Stokes channels
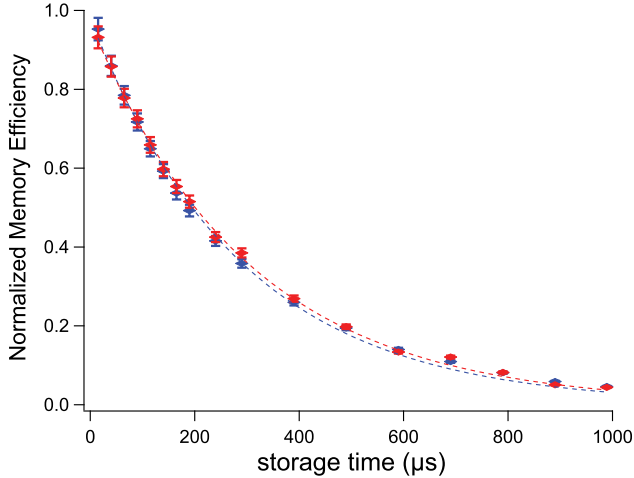
FIG. 3. (Color online) Dependence of retrieved signal [blue (dark gray)] and Stokes [red (light gray)] pulse energies as a function of storage time at $T = 70\,^\circ\text{C}$ ($\alpha_0 L = 52$). Here, $\tau_s = 300\ \mu$s. We normalized the memory efficiencies so that the zero-storage-time memory efficiency is unity. Experimentally, we were not operating under optimal storage conditions [17], and the zero-storage-time memory efficiency was $\approx 40\%$ for the signal pulse and $\approx 5\%$ for the Stokes pulse.

are representative of all experimental temperatures, although we found that the spin-wave decoherence rate does have an optical depth dependence.

III. THEORETICAL DESCRIPTION

A. Coupled propagation of signal and Stokes fields in a double-Λ system

In this section, we review the relevant theoretical description of the EIT-FWM process in a double-Λ interaction configuration. A single Λ link consisting of a strong control field (Rabi frequency Ω) and a weak signal field (Rabi frequency α) is usually considered in the context of light storage under EIT conditions. In such a single-Λ system under EIT conditions ($\nu - \nu_\text{c} \simeq \omega_\text{sg}$, where ν and ν_c are signal and control field frequencies, respectively), the control field enables strong coupling between the signal field and the long-lived atomic spin coherence that is usually described using the formalism of dark-state polaritons [14]. Adiabatic variation of the control field power reversibly transfers the signal optical field into the spin coherence, allowing for the realization of a quantum memory.

Achieving sufficiently high memory efficiency, however, requires operation with an atomic ensemble at high optical depth [15–17], where the effect on signal field propagation by the off-resonant interaction of the control field on the $|g\rangle$-$|e\rangle$ optical transition (Rabi frequency Ω') becomes significant and cannot be ignored. In particular, it results in the coherent creation of a Stokes field (frequency $\nu' = \omega_\text{es} - \Delta_\text{hf} - \delta$, Rabi frequency α') due to four-wave mixing (FWM). To properly account for this generation [6,9,10,12,20,23–32], it is necessary to take into account this off-resonant Λ link, which is shown in Fig. 1(a).

The rotating-frame Hamiltonian describing the atomic response to the light fields in such a configuration is

$$H/\hbar = -(\delta - \delta_s)|s\rangle\langle s| - (\delta - 2\delta_s)|e\rangle\langle e|$$
$$- \left[\alpha|e\rangle\langle g| + \Omega|e\rangle\langle s| + \frac{\Omega'\alpha'^*}{\Delta_\text{hf}}|s\rangle\langle g| + \text{H.c.}\right]. \quad (1)$$

Here, the Rabi frequencies of the signal and Stokes fields are $\alpha = E\mu/\hbar$ and $\alpha' = E'\mu'/\hbar$, where E and E' are the slowly varying envelopes of the signal and Stokes electric fields, respectively. μ and μ' are the real dipole matrix elements of the respective transitions. We define the optical polarization $P(z,t) = \rho_\text{eg}(z,t)\sqrt{N}$ and the spin coherence $S(z,t) = \rho_\text{sg}(z,t)\sqrt{N}$, where $\rho_{ij}(z,t)$ is the appropriate slowly varying position-dependent collective density matrix element and N is the number of atoms in the interaction volume. To derive Eq. (1), we used Floquet theory [33] to adiabatically eliminate the off-resonant interaction via Ω' and α'. To linear order in $1/\Delta_\text{hf}$ and in α', one obtains an effective Rabi frequency $\Omega'\alpha'^*/\Delta_\text{hf}$. States $|e\rangle$ and $|g\rangle$ acquire small light shifts $\delta_s = |\Omega'|^2/\Delta_\text{hf}$ and $-\delta_s$, respectively. For our Clebsch-Gordan coefficients [17], $\Omega' = -\sqrt{3}\Omega$. In order to match the equations of motion for quantum fields, we define $g\sqrt{N} = \sqrt{\gamma\alpha_0 c/2}$ as the coupling constant between the signal field and the atomic ensemble. We implicitly assume that the frequencies of the signal and Stokes fields are approximately the same, and we rescale the light field envelopes by defining dimensionless light field envelopes $\mathcal{E} = \frac{\mu}{\hbar g}E$ and $\mathcal{E}' = \frac{\mu}{\hbar g}E'$.

In the dipole approximation, assuming that, at all times, most of the atoms are in $|g\rangle$, and to linear order in the weak light fields $\mathcal{E}$ and $\mathcal{E}'$, the atomic evolution and light propagation equations read [11,12,20,23,25]

$$(\partial_t + c\partial_z)\mathcal{E} = ig\sqrt{N}P, \quad (2)$$

$$(\partial_t + c\partial_z)\mathcal{E}'^* = -ig\sqrt{N}\frac{\Omega}{\Delta_\text{hf}}S, \quad (3)$$

$$\partial_t S = -\Gamma_0 S + i\Omega P + i\frac{\Omega}{\Delta_\text{hf}}g\sqrt{N}\mathcal{E}'^*, \quad (4)$$

$$\partial_t P = -\Gamma P + i\Omega S + ig\sqrt{N}\mathcal{E}, \quad (5)$$

where we have defined $\Gamma_0 = \gamma_0 - i(\delta - \delta_s)$ and $\Gamma = \gamma - i(\delta - 2\delta_s)$. The polarization decay rate γ and the spin decay rate γ_0 have been introduced.

Equations (2)–(5) fully describe the propagation of the light fields and the dynamics of the spin wave and of the optical polarization during all stages of light storage. In the slow-light regime, when the control field is constant in time [$\Omega(t) = \Omega$], Eqs. (2)–(5) can be solved analytically using Fourier transformation in time [11,12,20,23,25]. In the stored-light regime, when the control field intensity is time-dependent, these equations can be solved numerically.

Figure 4 displays the results of storage experiments with 16-μs-long truncated Gaussian pulses at $T = 70\,^\circ\text{C}$ (optical depth $\alpha_0 L = 52$) along with the corresponding theoretical predictions, which are obtained by numerically solving Eqs. (2)–(5) with the appropriate parameters. We measured the control field power to be 4.7 mW, and the beam diameter was 2.67 mm, which corresponded to $\Omega/(2\pi) = 6.2$ MHz, and induced a light shift of $\delta_s = 17$ kHz. The spin-wave decay rate was measured to be approximately 300 μs, thus
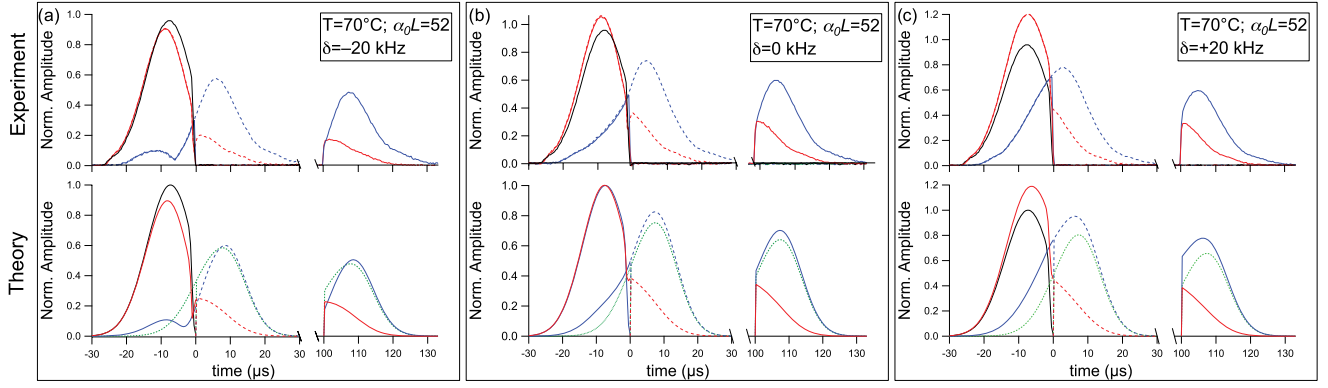
FIG. 4. (Color online) Storage and retrieval of 16-μs-long full width at half maximum (FWHM) truncated Gaussian pulses at $T = 70\,°\text{C}$ ($\alpha_0 L = 52$), for a two-photon detuning of (a) $\delta = -20$ kHz, (b) $\delta = 0$ kHz, and (c) $\delta = +20$ kHz. In all plots, the top graphs are experimental data and the bottom graphs are the theoretical predictions from Eqs. (2)–(5). The black curve is a far-detuned reference pulse, the blue (dark gray) traces are the signal pulses, and the red (light gray) traces are the Stokes pulses. Dashed (solid) lines correspond to slow- (stored-) light experiments. In the theory plots, the dotted green curve corresponds to a model consisting only of EIT to provide contrast with the EIT-FWM model. We scaled the pulses to the maximum amplitude of the reference pulse.

$\gamma_0/(2\pi) \approx 270$ Hz. The results from the slow-light experiment (dashed lines) and the stored-light experiment (solid lines) are overlaid to facilitate shape comparison.

For a small negative two-photon detuning $\delta = -20$ kHz [Fig. 4(a)], the signal field [in blue (dark gray)] experiences some distortion during propagation [as evidenced by the bumps in the leakage portion of the pulse (when $t < 0$), which exits the cell before the control field is extinguished], but the shape of the slow pulse is preserved during the storage process. Likewise, the fraction of the Stokes field that exits the medium at $t > 0$ in the slow-light experiment [dashed red (light gray)] matches the retrieved Stokes field in the stored-light experiment [solid red (light gray)]. There is an excellent agreement between the experimental observations and the numerical model predictions. The dotted green trace in the theory plot corresponds to standard EIT-based light storage of the signal field, where the FWM process has been artificially turned off. To compute this trace, the Stokes contribution in Eq. (4) is set to zero, and Eqs. (2), (4), and (5) are solved numerically. We include this trace in order to showcase the effects of four-wave mixing on signal pulse shape and delay.

Figure 4(b) demonstrates the excellent correspondence between experiment and theory for a two-photon detuning of $\delta = 0$ kHz. For this value of δ, the signal pulse is less distorted during propagation, but the pulse shape is still distinct from the bare-EIT model. Likewise, Fig. 4(c) depicts the results for $\delta = +20$ kHz $\approx \delta_s$, where the two-photon detuning effectively cancels the light shift during the writing and retrieval stages. Under this condition, the signal pulse will experience the least amount of distortion due to FWM, since the EIT transmission peak is, at least for a sufficiently narrow pulse bandwidth, symmetric about $\delta = \delta_s$. As a result, the dispersion experienced by the pulse is mostly linear. In all cases, the theoretical model matches the experimental data very well.

The correspondence between slow-light pulse shapes (dashed lines) and the shapes of the retrieved pulses (solid lines) illustrates an important result— when the writing and retrieval control field amplitudes are constant in time, the

process of switching the control field off and on has little effect on the signal and Stokes fields, apart from a delay and the spin-wave decay during storage time. In this case, we can further understand the effects of FWM by using the closed-form solutions to the Fourier transformed versions of Eqs. (2)–(5) [11,12,20,23]. In the appendix, we detail the derivation of the following two approximate equations, which intuitively describe the effects of FWM and EIT on pulse propagation for the case $\delta = \delta_s$. Although these equations make a set of strong assumptions, including the assumption of an infinitely wide EIT transmission window $\Gamma_E \to \infty$, they preserve the essential physics in the limit of weak FWM. Defining $\Delta_{\text{R}} = -\Omega^2/\Delta_{\text{hf}}$, the equations are

$$\mathcal{E}(L,t) \approx \mathcal{E}(0, t - L/v_g) + \Delta_{\text{R}}^2 \int_0^{L/v_g} dt'\, \mathcal{E}(0, t - t')t'$$

$$+ i\,\Delta_{\text{R}} \int_0^{L/v_g} dt'\, \mathcal{E}'^*(0, t - t'), \qquad (6)$$

$$\mathcal{E}'^*(L,t) \approx \mathcal{E}'^*(0,t) + \Delta_{\text{R}}^2 \int_0^{L/v_g} dt'\, \mathcal{E}'^*(0, t - t')(L/v_g - t')$$

$$- i\,\Delta_{\text{R}} \int_0^{L/v_g} dt'\, \mathcal{E}(0, t - t'). \qquad (7)$$

These equations clearly show how the effects of FWM grow with optical depth $\alpha_0 L$. The first term on the right-hand side (RHS) of Eq. (6) describes the delay that the signal field experiences during propagation in an EIT medium, where $v_g = 2\Omega^2/(\alpha_0 \gamma)$ is the EIT group velocity [13]. Due to the effects of FWM, the signal field acquires a small in-phase gain of order $\Delta_{\text{R}}^2 (L/v_g)^2 \sim (\alpha_0 L)^2 \gamma^2/\Delta_{\text{hf}}^2$ from times up to L/v_g earlier. The times farthest away are weighted more heavily. Additionally, the signal field acquires an i-out-of-phase contribution of order $|\Delta_{\text{R}}|L/v_g \sim \alpha_0 L\gamma/\Delta_{\text{hf}}$ from the Stokes field up to L/v_g earlier with all times contributing equally. The Stokes field propagates undistorted and largely undelayed, but gets a small [order $(\alpha_0 L)^2\gamma^2/\Delta_{\text{hf}}^2$] in-phase gain from times up to L/v_g earlier, with closest times weighted more heavily, and also an i-out-of-phase contribution of order $\alpha_0 L\gamma/\Delta_{\text{hf}}$ from the signal field, with all times weighted

equally. Notice that, in both equations, in the regime where the first term on the RHS is large, small in-phase $(\alpha_0 L)^2 \gamma^2 / \Delta_{\mathrm{hf}}^2$ terms and small i-out-of-phase $\alpha_0 L \gamma / \Delta_{\mathrm{hf}}$ terms contribute at the same $(\alpha_0 L)^2 \gamma^2 / \Delta_{\mathrm{hf}}^2$ order to the absolute value of the field (which is what our experiment measures).

However, the first terms on the RHS are not always dominant. In particular, for $t > 0$, the first term on the RHS of Eq. (7) vanishes, in which case $|\mathcal{E}'^*(L,t)|$ is dominated by the third term with a small correction from the second term. This means, as we will confirm experimentally, that the retrieved Stokes field is largely determined by the input signal, and not by the input Stokes field. Similarly, if EIT group delay is comparable to the signal pulse duration, then, for $t < 0$, the RHS of Eq. (6) is small and $|\mathcal{E}(L,t)|$ is significantly affected by the third term. This means, as we will confirm experimentally, that the signal pulse leakage can be strongly affected by the Stokes input, in contrast to the retrieved signal pulse, which is only weakly affected by the Stokes input. Equations (6) and (7) also show that the perturbative treatment of the effects of FWM, employed to derive them, breaks down when $|\Delta_{\mathrm{R}} L / v_g| \gtrsim 1$; that is, when the optical depth is $\alpha_0 L \gtrsim 2\Delta_{\mathrm{hf}}/\gamma \approx 100$.
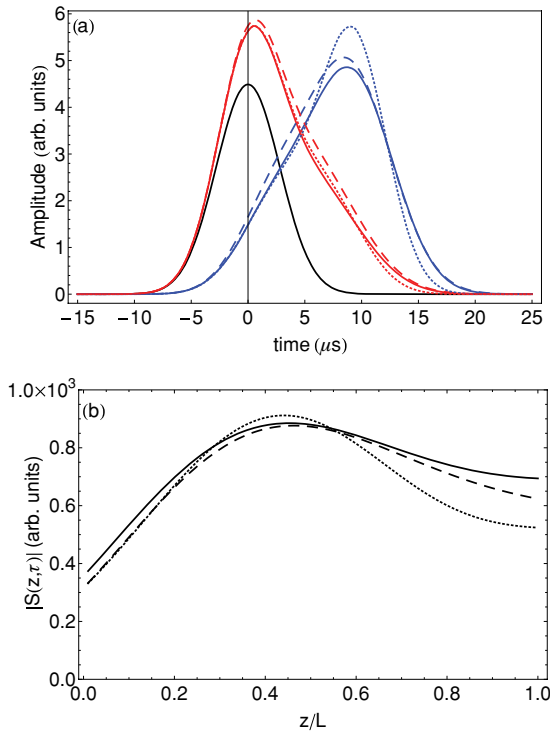

FIG. 5. (Color online) (a) Results of a numerical investigation of slow light with a 6.6-μs-long pulse (reference in black), with $\Omega/(2\pi) = 10$ MHz and $\alpha_0 L = 80$, so that the bandwidth of the pulse $\Delta\omega = 0.1\Gamma_{\mathrm{E}}$. Blue (dark gray) traces are the signal field; red (light gray) traces are the Stokes field. Solid lines are the result of numerically solving Eqs. (2)–(5). Dotted lines are the result of the infinite-Γ_{E} approximation in Eqs. (6)–(7). Dashed lines correspond to results obtained using numerical integration of expressions in Eqs. (A4), (A5), (A11)–(A15) in the appendix. (b) Spin wave created at time $\tau = 5$ μs delay in Fig. 5(a). The solid black line is the result of numerically solving Eqs. (2)–(5). Dotted lines are the results from Eq. (15). Dashed lines are the results from Eqs. (A17) and (A23).

To test the validity of Eqs. (6) and (7), in Fig. 5(a) we compare the solutions obtained by numerically solving Eqs. (2)–(5) (solid lines) to the predictions of Eqs. (6) and (7) (dotted lines). In the dashed traces, we include the results of a useful intermediate approximation, which does not assume infinite Γ_{E} and is described by Eqs. (A4), (A5), (A11)–(A15) in the appendix. For these plots, $\Omega/(2\pi) = 10$ MHz and $\alpha_0 L = 80$; the pulse bandwidth was $\Delta\omega = 0.1\Gamma_{\mathrm{E}}$. From the excellent correspondence between theoretical models, it is evident that the approximations made in deriving Eqs. (6) and (7) are valid.

B. Effect of four-wave mixing on the spin wave

While the solutions of Eqs. (2)–(5) accurately describe the evolution of light pulses and atomic variables under slow-light and storage conditions, we have not yet used them to elucidate the role that the Stokes field plays in the creation of the spin coherence. Specifically, it is not yet clear whether the quantum memory description based on the dark state polariton principle [14] is valid under EIT-FWM conditions. In what follows, we develop a more transparent description of light storage in a double-Λ system and show that, in this case, the spin wave is determined by a particular combination of signal and Stokes fields.

We obtain this result by adiabatically eliminating the optical polarization $P(z,t)$. We set the time derivative to zero in Eq. (5) and find

$$P(z,t) \approx i\frac{\Omega}{\Gamma}S(z,t) + i\frac{g\sqrt{N}}{\Gamma}\mathcal{E}(z,t). \quad (8)$$

Inserting Eq. (8) into Eq. (4), we obtain the following equation for time evolution of the spin wave $S(z,t)$:

$$\partial_t S(z,t) = -\left(\Gamma_0 + \frac{\Omega^2}{\Gamma}\right)S(z,t) - g\sqrt{N}\frac{\Omega}{\Gamma}\mathcal{F}(z,t). \quad (9)$$

It is easy to see that the spin wave depends only on a combination $\mathcal{F}(z,t)$ of the signal and Stokes optical fields, defined as

$$\mathcal{F}(z,t) = \mathcal{E}(z,t) - i\frac{\Gamma}{\Delta_{\mathrm{hf}}}\mathcal{E}'^*(z,t). \quad (10)$$

Equation (9) is analogous to the spin-wave expression obtained through a similar treatment of a standard three-level light storage model [14],

$$\partial_t S(z,t) = -\left(\Gamma_0 + \frac{\Omega^2}{\Gamma}\right)S(z,t) - g\sqrt{N}\frac{\Omega}{\Gamma}\mathcal{E}(z,t), \quad (11)$$

but with one modification—the single light field (signal) is now replaced by a combined signal-Stokes field $\mathcal{F}$. Thus, one might expect that it should be possible to store information about this joint mode in the spin coherence. However, only a small $(\alpha_0 L)^2 \gamma^2 / \Delta_{\mathrm{hf}}^2$ fraction of the Stokes field [the second term on the RHS of Eq. (7)] exits the medium at $t > 0$ after the input Stokes has been turned off, while the signal pulse is delayed in its entirety [the first term on the RHS of Eq. (6)]. As a result, in contrast to the information encoded in the signal field, most of the information encoded in the Stokes field is lost to leakage, which leaves the interaction region before the control field is shut off.

The similarity between Eqs. (9) and (11) motivates a more detailed comparison of our EIT-FWM system with the traditional EIT configuration. The propagation equation for $\mathcal{F}$ is easily obtained from the appropriate combination of Eqs. (2) and (3):

$$(\partial_t + c\partial_z)\mathcal{F} = -\frac{g^2 N}{\Gamma}\mathcal{F} - \Omega\frac{g\sqrt{N}}{\Gamma}S - i\frac{g^2 N}{\Delta_{\text{hf}}}\mathcal{E}'^*. \qquad (12)$$

This equation is also similar to the signal propagation expression in the classic stored-light model [14],

$$(\partial_t + c\partial_z)\mathcal{E} = -\frac{g^2 N}{\Gamma}\mathcal{E} - \Omega\frac{g\sqrt{N}}{\Gamma}S, \qquad (13)$$

except for the optical-depth-dependent Stokes term, which describes the generation of signal from Stokes during propagation through a sufficiently optically-thick medium.

When the two-photon detuning is chosen such that the light shift is canceled (i.e., $\delta = \delta_s$), the propagation equation becomes, to $O(1/\Delta_{\text{hf}})$,

$$\left[\partial_t + c\cos^2\theta(t)\partial_z\right]\mathcal{F}(z,t) \approx i\Delta_{\text{R}}\mathcal{E}'^*(z,t), \qquad (14)$$

with the angle $\theta(t)$ given by $\tan^2\theta(t) = \frac{g^2 N}{\Omega^2(t)}$.

Analysis of above equations demonstrates two regimes for light storage under EIT-FWM conditions. At low optical depths, the contribution of the Stokes field on the RHS of Eqs. (12) and (14) is negligible. In this case, the equations for the joint field $\mathcal{F}$ and spin wave S become identical to those for $\mathcal{E}$ and S in the regular EIT configuration. For example, if we replace the RHS of Eq. (14) with zero, it would describe the propagation of $\mathcal{F}$ without distortion at a reduced group velocity $v_g = c\cos^2\theta \approx \frac{2\Omega^2}{\alpha_0\gamma}$. However, at low optical depths and $t > 0$ (after the input Stokes pulse has been turned off), the contribution of the Stokes field into $\mathcal{F}$ is also negligible: it is small not only because of the small factor $\Gamma/\Delta_{\text{hf}}$ in Eq. (10) but also because $\mathcal{E}'(z,t)$ itself is small [since the first term on the RHS of Eq. (7), generalized to arbitrary z, vanishes for $t > 0$]. Thus, signal field propagation can be analyzed using a three-level single Λ, even though the Stokes field can be significantly affected by control and signal fields, as is evident from the dominance of the last term on the RHS of Eq. (7) for $t > 0$.

However, at higher optical depths, the term on the RHS of Eq. (14) becomes significant. Specifically, this term results in gain or loss of the signal field due to the Stokes field. The dashed blue (dark gray) lines in Fig. 6 depict the results of numerical calculations of the homogeneous form of Eq. (14). Solid blue (dark gray) lines show the results of the numerical evaluation of the full form of Eq. (14) with Eqs. (3) and (9). For these calculations, $\Omega/(2\pi) = 8$ MHz, $\gamma/(2\pi) = 150$ MHz, and the signal pulse was chosen so that its bandwidth $\Delta\omega = 0.05\Gamma_{\text{E}}$. It is evident from this graph that the Stokes contribution is not negligible for optical depths $\alpha_0 L \gtrsim 25$, when the simple slow propagation of $\mathcal{F}$ breaks down due to the Stokes term on the RHS of Eq. (14).
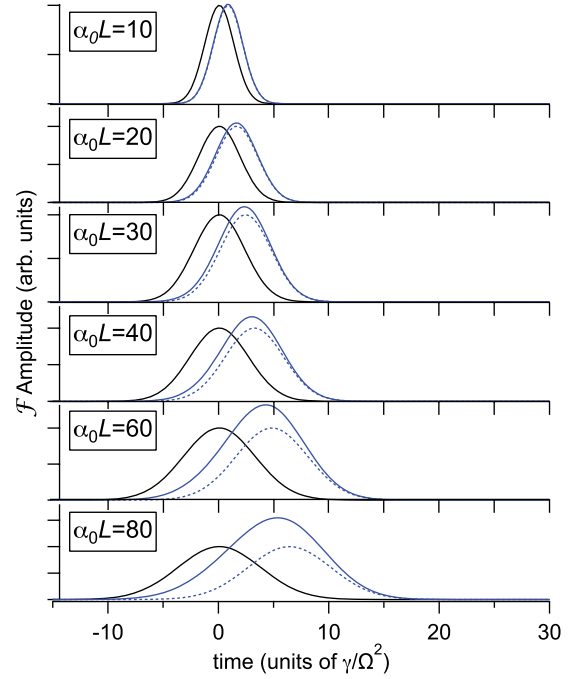

FIG. 6. (Color online) Results from numerical evaluation of Eqs. (3), (9), and (14) [solid blue (dark gray) lines] and of the homogeneous version of Eq. (14) [dashed blue (dark gray) lines] for a range of optical depths $\alpha_0 L$, as indicated in the legends. The bandwidth of each input pulse was $\Delta\omega = 0.05\Gamma_{\text{E}} = \Omega^2/(20\sqrt{\alpha_0 L/2}\gamma)$.

As shown in the appendix, the same approximations that lead to Eqs. (6) and (7) give the following expression for the spin wave $S(z,t)$ in the limit when $\Gamma_{\text{E}} \to \infty$:

$$S(z,t) \approx -\frac{g\sqrt{N}}{\Omega}\left[\mathcal{E}\left(0,t-\frac{z}{v_g}\right) + \Delta_{\text{R}}^2\int_0^{\frac{z}{v_g}}dt'\mathcal{E}(0,t-t')t'\right.$$
$$\left. + i\Delta_{\text{R}}\int_0^{\frac{z}{v_g}}dt'\mathcal{E}'^*(0,t-t')\right]. \qquad (15)$$

In Fig. 5(b), we compare the shape of the spin wave that is obtained by numerically solving Eqs. (2)–(5) (solid lines) to the predictions of Eq. (15) (dotted lines). As in Fig. 5(a), we also include the predictions of an intermediate approximation, which does not assume an infinite Γ_{E} and is described in Eqs. (A17) and (A23) in the appendix. The reasonable agreement between the three curves in Fig. 5(b) implies that Eq. (15) does indeed contain the essential physics. In particular, under this approximation, the spin wave is proportional to the signal field only, as in a traditional three-level single-Λ EIT system [see Eq. (A23) in the appendix],

$$S(z,t) \approx -\frac{g\sqrt{N}}{\Omega}\mathcal{E}(z,t). \qquad (16)$$

Moreover, under this approximation, $\mathcal{E}(z,t)$ [and hence $S(z,t)$] is mostly determined by the usual slowed-down version of the input signal [first term in the square brackets in Eq. (15)] with small corrections of order $|\Delta_{\text{R}}|L/v_g \sim \alpha_0 L\gamma/\Delta_{\text{hf}}$ [third term in square brackets in Eq. (15)] and $(\alpha_0 L)^2\gamma^2/\Delta_{\text{hf}}^2$ [second term in square brackets in Eq. (15)].
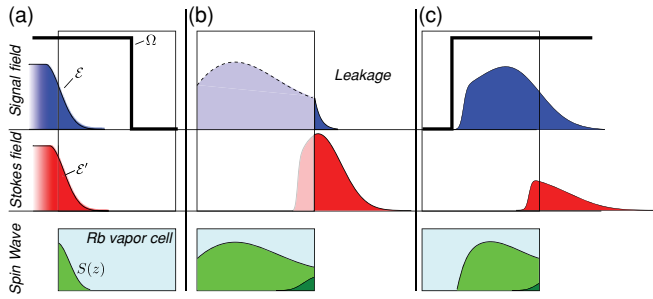
FIG. 7. (Color online) Illustration of the modified storage description. (a) During the writing stage, the input signal field $\mathcal{E}$ (top) and Stokes field $\mathcal{E}'$ (middle) propagate at different group velocities through the atomic medium, creating a spin wave (bottom). (b) During the storage stage, the control field is turned off and no light fields are present. Some portion of the signal field has propagated through the cell and leaks out before the control field is extinguished. At the same time, most of the information in the Stokes field is lost in the leakage, since, in the regime $(\alpha_0 L)\gamma/\Delta \ll 1$, the propagation of the Stokes field is affected by the atoms only weakly [see Eq. (7)]. The spin wave is preserved during storage. (c) During retrieval, the control field is turned on, releasing the spin wave into both the signal and Stokes fields, which exit the vapor cell.

Figure 7 illustrates an intuitive way to understand storage under EIT-FWM conditions. At the beginning of the writing stage, shown in Fig. 7(a), the control field (in black) prepares the atoms and causes the input signal field $\mathcal{E}$ (in blue, top) to propagate at a reduced group velocity. The Stokes pulse (in red, middle) enters the cell and is not completely extinguished inside the medium even after the reference pulse would have left the medium. A collective spin coherence is created in the atomic vapor cell (in green, bottom). As the pulses propagate through the atomic medium, as shown in column (b), they experience mutual interference effects and may become distorted. The spin wave propagates along with the signal field. The contributions to the spin wave are determined by the joint mode $\mathcal{F}$, and we can distinguish between the contributions to the spin wave from the signal field (shown in light green) and those of the Stokes field (shown in dark green) [see Eq. (15)]. In the regime of weak FWM, the propagation of the Stokes field is only weakly affected by the atoms [see Eq. (7)], so that much of the Stokes field leaves the end of the vapor cell as leakage. Any information contained in this leaked field is lost for the storage process, which commences when the control field is shut down. After some time [column (c)], the control field is turned on, and the spin wave is released into both the signal and Stokes fields. It is important to note that, since the joint mode $\mathcal{F}$ is not a normal mode, the proportion of Stokes to signal is not fixed.

In the regime of weak FWM ($\alpha_0 L \leqslant 25$), the joint mode $\mathcal{F}(z,t)$ is determined mostly by the input signal field $\mathcal{E}$. Thus, the propagation dynamics experienced by the signal pulse will be only slightly sensitive to the amplitude of the seeded Stokes pulse [of order $\alpha_0 L \gamma/\Delta_{hf}$, see the last term in Eq. (6)], and consequently the spin wave created will have the same weak dependence on the seeded Stokes field [see the last term in Eq. (15)]. Since the spin wave is only weakly dependent on the input Stokes field, it is possible to create approximately the same spin wave for different input combinations of signal and
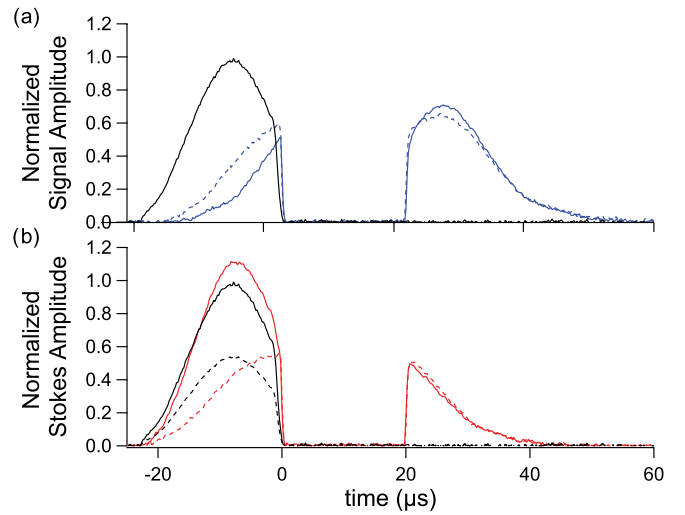

FIG. 8. (Color online) Storage of a 15 μs (FWHM) truncated Gaussian pulse at $T = 70\,^{\circ}$C ($\alpha_0 L = 52$) under different Stokes seeding conditions. Solid lines depict storage when the Stokes seed amplitude is the same as the signal amplitude. The dashed lines correspond to the case of a reduced input Stokes field. The black traces show reference (input) pulses, and the dashed black trace in the bottom plot illustrates the reduced Stokes seed amplitude. We scaled the pulses to the maximum amplitude of the reference pulse for the case of the full Stokes seed.

Stokes fields. The retrieval from the spin wave into the light fields will consequently have this same weak dependence on the input Stokes field.

Equations (6) and (7) support this conclusion. Specifically, the amplitude of the retrieved signal field [Eq. (6)] is determined primarily by the input signal field (the first term on the RHS) with a small $(\alpha_0 L\gamma/\Delta_{hf})^2$ correction from the input Stokes field (the third term on the RHS). Similarly, since the first term on the RHS of Eq. (7) vanishes for $t > 0$, the retrieved Stokes field is also determined primarily by the input signal (the third term on the RHS) with a small $(\alpha_0 L\gamma/\Delta_{hf})^2$ correction from the input Stokes (the second term on the RHS). At the same time, signal and Stokes outputs are more strongly affected by the Stokes input for $t < 0$ (leaked pulses) than for $t > 0$ (retrieved pulses). This statement is obvious for the Stokes field, since the first term on the RHS of Eq. (7) does not vanish for $t < 0$. The reason this statement holds for the output signal is that the first term on the RHS of Eq. (6) is smaller for $t < 0$ than for $t > 0$ for a sufficiently large group delay, while the third term on the RHS of Eq. (6) is larger for $t < 0$ than for $t > 0$ since $\mathcal{E}'(0, t-t')$ vanishes for $t - t' > 0$.

In Fig. 8, we display the results of an experiment designed to test these conclusions. The top graph [Fig. 8(a)] depicts the storage of a 15-μs-long (FWHM) truncated Gaussian signal field at $T = 70\,^{\circ}$C ($\alpha_0 L = 52$). The solid trace corresponds to approximately equal amplitudes of input signal and Stokes optical pulses, while the dashed traces correspond to a reduced initial Stokes amplitude $\mathcal{E}'^*(0, t) = -0.55\mathcal{E}(0, t)$.

Notice the difference in the leakage portion ($t < 0$) of both the signal pulse and the Stokes pulse as we go from solid curves to dashed curves, which exemplifies that both signal and
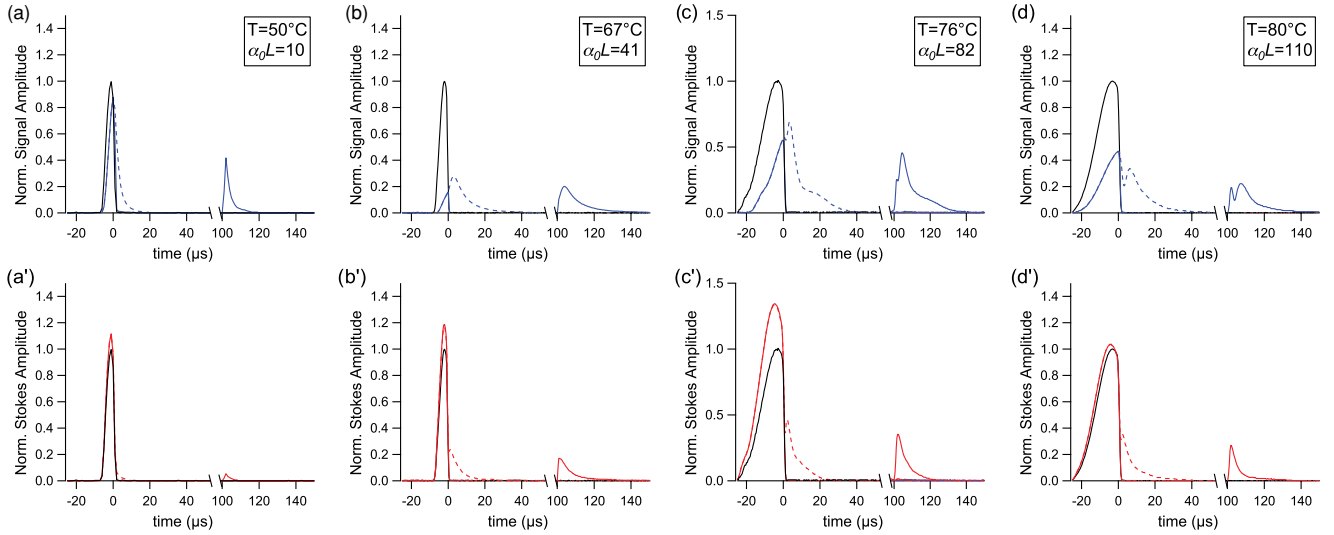
FIG. 9. (Color online) Stokes behavior for increasing optical depths. For all cases, the two-photon detuning $\delta = 0$. The black trace is a reference pulse; the blue (dark gray) [red (light gray)] trace is the signal (Stokes) pulse. (a), (a′) Storage and retrieval of a 6-μs-long (FWHM) truncated Gaussian pulse at $T = 50\,^{\circ}$C, which corresponds to an optical depth of $\alpha_0 L = 10$. Here, $\Omega/(2\pi) = 8.3$ MHz. (b), (b′) $T = 67\,^{\circ}$C ($\alpha_0 L = 41$), pulse duration is 6 μs, $\Omega/(2\pi) = 7.1$ MHz. (c), (c′) $T = 76\,^{\circ}$C ($\alpha_0 L = 82$), pulse duration is 20 μs, $\Omega/(2\pi) = 12.7$ MHz. (d), (d′) $T = 80\,^{\circ}$C ($\alpha_0 L = 110$), pulse duration is 20 μs, $\Omega/(2\pi) = 7.8$ MHz. We scaled the pulses to the maximum amplitude of the reference pulse.

Stokes outputs for $t < 0$ do depend strongly on the amplitude of the seeded Stokes pulse, as we have explained theoretically above and as we have reported previously [12]. At the same time, the retrieved ($t > 0$) Stokes and signal pulses are both almost independent of the amplitude of the seeded Stokes field, which is consistent with the theoretical explanation above. We repeated similar measurements many times under a wide range of experimental conditions and found the retrieved pulses to be weakly affected by the seeded Stokes amplitude as long as the input signal field is comparable to or stronger than the input Stokes field.

IV. OPTICAL DEPTH DEPENDENCE OF THE STOKES FIELD

In this section, we present the results of storage experiments at increasing optical depths.

Figure 9 depicts the evolution of the Stokes and signal fields under storage conditions as the optical depth increases. The general features of these results are well explained by the simple signal and Stokes expressions in Eqs. (6) and (7), as described below. In Figs. 9(a) and 9(a′), we show the results of slow-light and stored-light experiments using a 6-μs-long (FWHM) truncated Gaussian pulse at a temperature of $T = 50\,^{\circ}$C, which corresponds to an optical depth of $\alpha_0 L = 10$. The signal pulse [blue (dark gray) trace in Fig. 9(a)] experiences a reduction in group velocity during propagation, as seen by comparing the dashed trace (slow light) to the black trace, which is a far-detuned reference pulse. The Stokes pulse [red (light gray) trace in Fig. 9(a′)] closely mimics the far-detuned reference pulse, indicating that four-wave mixing is not a dominant process at this optical depth. In a separate run, we investigate storage of these pulses by turning off the control field for 100 μs. Upon retrieval, the signal field

[solid blue (dark gray) trace in Fig. 9(a)] is recovered with a modest reduction in amplitude due to spin-wave decay during the storage time, but its shape is preserved. Additionally, we retrieve a small pulse on the Stokes channel [solid red (light gray) trace in Fig. 9(a′)]. Equation (6) predicts that, at low optical depths [$(\alpha_0 L \gamma / \Delta_{\mathrm{hf}}) \ll 1$], the retrieved signal pulse will be a delayed version of the input pulse (if one accounts for the storage time), but with a slight modification due to the Stokes field [the last term in Eq. (6)]. Likewise, the Stokes field will be mostly unaffected by the atoms [the first term on the RHS of Eq. (7)], so most of it will leak out (see $t < 0$). However, a small Stokes pulse $\propto (\alpha_0 L / \Delta_{\mathrm{hf}})$ generated from the input Signal [the last term in Eq. (7)] will be retrieved.

Figures 9(b) and 9(b′) show the results of similar experiments at $T = 67\,^{\circ}$C, corresponding to an optical depth of $\alpha_0 L = 41$. Here, the signal shape is again preserved by the storage process. The four-wave mixing effects are exhibited by the Stokes gain in the leakage portion of the pulse [see Fig. 9(b′)], which leaves the interaction region before the storage stage occurs. This gain is described by the last two terms in Eq. (7). At this increased optical depth, the last term in Eq. (7) also predicts an increased Stokes output for $t > 0$. The effects of FWM are also apparent in the distortion that the signal field experiences during propagation.

Figures 9(c) and 9(c′) depict the storage experiments at $T = 76\,^{\circ}$C ($\alpha_0 L = 82$). We used a longer pulse (FWHM of 20 μs). At this optical depth, the Stokes pulse experiences more gain during propagation. Storage and retrieval, however, still preserve the shapes of both the signal and the Stokes pulse. Again, it is clear that the Stokes field gain predicted by Eq. (7) becomes more apparent at higher optical depths. We also see that, at $\alpha_0 L = 110$ [column (d)], the Stokes field amplitude is smaller than at $\alpha_0 L = 82$ [column (c)]. This effect is most likely due to the absorption of the control field by unprepared

atoms that enter the interaction region during the waiting time. We also note that, at $\alpha_0 L \approx 100$, the perturbative expansion used to derive Eqs. (6) and (7) breaks down.

V. CONCLUSION

We have studied the phenomenon of stored light under conditions of electromagnetically induced transparency (EIT) and four-wave mixing (FWM) in an ensemble of hot Rb atoms. In particular, we have investigated the prospect of simultaneously storing both a signal and a Stokes pulse in a single atomic coherence and have shown that independent storage of two modes is not possible. The reason is that most of the Stokes pulse leaks out of the medium during the writing stage, so that, during retrieval, both output fields are determined primarily by the input signal field and depend on the input Stokes field only very weakly.

We presented a theoretical model based on a simple double-Λ system, which agreed very well with experimental observations. This model allowed us to derive a simple relationship between input and output fields, which explained the above mentioned impossibility of two-mode storage. Furthermore, we showed that a particularly convenient description of storage

in an EIT-FWM system involves a joint signal-Stokes mode, whose dynamics we also studied. Quantum properties of our system will be investigated in the future using the analysis similar to that in Refs. [30–32].

APPENDIX: DERIVATION OF EQS. (6), (7), (15), AND (16)

In the main text, we omitted the derivations of Eqs. (6), (7), (15), and (16). In this appendix, we present these derivations.

Since experiments and numerics show that turning the control field off and back on has a negligible effect on the fields except for a delay and spin-wave decay during the storage time, we solve Eqs. (2)–(5) in the main text assuming a constant control field. In the comoving frame $(\partial_t + c\partial_z \to c\partial_z)$ and by Fourier transforming in time $(t \to \omega$ and $\partial_t \to -i\omega)$, Eqs. (2)–(5) can be written as

$$\partial_z \begin{pmatrix} \mathcal{E}(z,\omega) \\ \mathcal{E}'^*(z,\omega) \end{pmatrix} = i\frac{\alpha_0\gamma}{2F} \begin{pmatrix} \omega + i\Gamma_0 & -\frac{\Omega^2}{\Delta_{\rm hf}} \\ \frac{\Omega^2}{\Delta_{\rm hf}} & -\frac{\Omega^2}{\Delta_{\rm hf}^2}(\omega + i\Gamma) \end{pmatrix} \begin{pmatrix} \mathcal{E}(z,\omega) \\ \mathcal{E}'^*(z,\omega) \end{pmatrix} = M \begin{pmatrix} \mathcal{E}(z,\omega) \\ \mathcal{E}'^*(z,\omega) \end{pmatrix}, \tag{A1}$$

where $F = \Omega^2 + (\Gamma - i\omega)(\Gamma_0 - i\omega)$ (see Eq. (2) in Ref. [12]).

To gain some intuition for how FWM may result in amplification, one can consider a simple case, in which the diagonal terms in the matrix M in Eq. (A1) vanish (equivalently, one could consider the case where the Stokes field also propagates in its own EIT medium). Approximating further $F \to \Omega^2$, we find that

$$M \approx i\frac{\alpha_0\gamma}{2\Delta_{\rm hf}} \begin{pmatrix} 0 & -1 \\ 1 & 0 \end{pmatrix} \tag{A2}$$

and has eigenvectors $(1, \pm i)$ with eigenvalues $\pm\frac{\alpha_0\gamma}{2\Delta_{\rm hf}}$, corresponding to an exponentially growing solution and an

exponentially decaying solution. In our experiment, however, the diagonal terms for the signal and the Stokes fields are very different. Moreover, the effect of FWM is rather small and can, in fact, be treated perturbatively, as we will show below.

We checked numerically that the last entry in the matrix M in Eq. (A1) does not significantly affect our results. For example, it gives a contribution to $\mathcal{E}'(L,\omega)$ of order $\alpha_0 L \gamma^2/\Delta_{\rm hf}^2$, which will be negligible relative to other contributions of order $(\alpha_0 L)^2\gamma^2/\Delta_{\rm hf}^2$ since $\alpha_0 L \gg 1$. We will therefore neglect the last entry in the matrix M in Eq. (A1) for the rest of this appendix.

Equation (A1) can then be solved to give [11,12,20,23,25]

$$\begin{pmatrix} \mathcal{E}(z,\omega) \\ \mathcal{E}'^*(z,\omega) \end{pmatrix} = e^{i\sigma z} \begin{pmatrix} \cosh(\xi z) + i\frac{\sigma}{\xi}\sinh(\xi z) & i\frac{2\Delta_{\rm R}}{\beta}\sinh(\xi z) \\ -i\frac{2\Delta_{\rm R}}{\beta}\sinh(\xi z) & \cosh(\xi z) - i\frac{\sigma}{\xi}\sinh(\xi z) \end{pmatrix} \begin{pmatrix} \mathcal{E}(0,\omega) \\ \mathcal{E}'^*(0,\omega) \end{pmatrix}, \tag{A3}$$

where $\Delta_{\rm R} = -\Omega^2/\Delta_{\rm hf}$, $\beta = \sqrt{(\Gamma_0 - i\omega)^2 + 4\Delta_{\rm R}^2}$, $\sigma = \frac{\alpha_0\gamma}{4F}(i\Gamma_0 + \omega)$, and $\xi = \frac{\alpha_0\gamma}{4F}\beta$.

Using the convolution theorem, we then obtain

$$\mathcal{E}(z,t) = \int dt' \mathcal{E}(0,t-t') f_1(z,t') + \int dt' \mathcal{E}(0,t-t') f_2(z,t') + \int dt' \mathcal{E}'^*(0,t-t') f_3(z,t'), \tag{A4}$$

$$\mathcal{E}'^*(z,t) = \mathcal{E}'^*(0,t) + \int dt' \mathcal{E}'^*(0,t-t') g_2(z,t') + \int dt' \mathcal{E}(0,t-t') g_3(z,t'), \tag{A5}$$

where

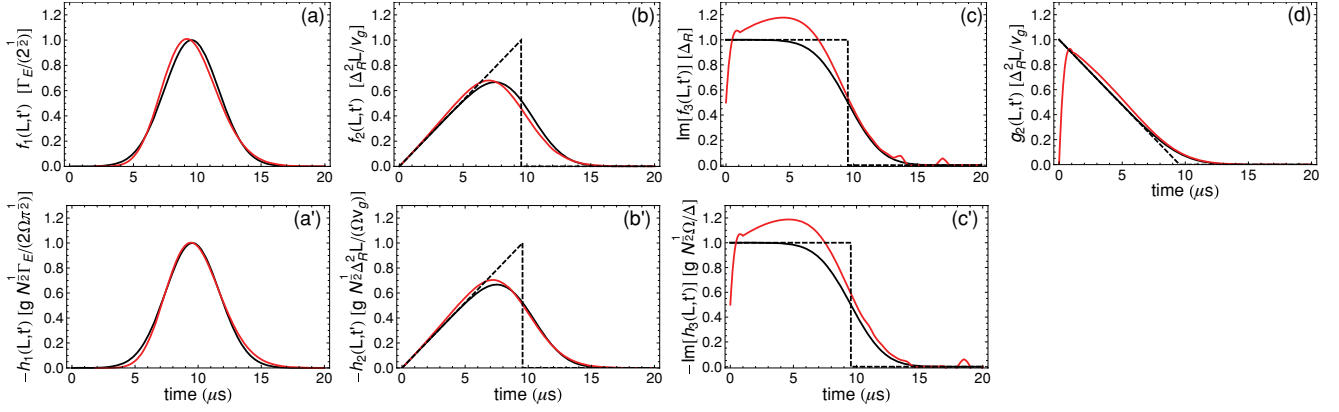$$f_1(z,t') = \frac{1}{2\pi}\int d\omega e^{2i\sigma z}e^{-i\omega t'}, \tag{A6}$$

FIG. 10. (Color online) Graphs of (a) $f_1(L,t)$, (a') $-h_1(L,t)$, (b) $f_2(L,t)$, (b') $-h_2(L,t)$, (c) $\text{Im}[f_3(L,t)] = -\text{Im}[g_3(L,t)]$, (c') $-\text{Im}[h_3(L,t)]$, and (d) $g_2(L,t)$. For the calculations, $\Omega/(2\pi) = 10$ MHz, $\alpha_0 L = 80$. Red curves show the result of numerical integration of the respective expression in Eqs. (A6)–(A10), (A18)–(A20). Solid black curves show the approximate forms of the integrals given in Eqs. (A11)–(A15), (A23), without taking the limit $\Gamma_E \to \infty$. The dashed black curves incorporate the $\Gamma_E \to \infty$ approximations in Eqs. (A11)–(A15), (A23).

$$f_1(z,t') + f_2(z,t') = \frac{1}{2\pi} \int d\omega e^{i\sigma z} \left[\cosh(\xi z) + i\frac{\sigma}{\xi} \sinh(\xi z) \right] e^{-i\omega t'}, \tag{A7}$$

$$f_3(z,t') = \frac{1}{2\pi} \int d\omega e^{i\sigma z} i\frac{2\Delta_R}{\beta} \sinh(\xi z) e^{-i\omega t'}, \tag{A8}$$

$$\delta(t') + g_2(z,t') = \frac{1}{2\pi} \int d\omega e^{i\sigma z} \left[\cosh(\xi z) - i\frac{\sigma}{\xi} \sinh(\xi z) \right] e^{-i\omega t'}, \tag{A9}$$

$$g_3(z,t') = -f_3(z,t'). \tag{A10}$$

Here, f_1 and f_2 are defined in such a way that f_1 captures pure EIT, while f_2 describes how FWM changes the relationship between the input signal and the output signal. f_3 describes the effect of the input Stokes field on the output signal. Similarly, the first term in Eq. (A5) describes pure undistorted propagation of the Stokes field in the absence of FWM. g_2 describes how FWM changes the relationship between the input Stokes field and the output Stokes field. Finally, g_3 describes the effect of the input signal on the output Stokes field.

To get some insight into the behavior of f_i and g_i, we consider the case $\delta = \delta_s$ (generalization to arbitrary δ is straightforward). We further take the limit $\gamma_0 = 0$, which is a reasonable approximation in our experiment, except during the waiting time between writing and retrieval (however, again one can easily generalize the derivation below to $\gamma_0 \neq 0$). Furthermore, we expand f_2 and g_2 to second order in $1/\Delta_{\text{hf}}$ and expand f_3 and g_3 to first order in $1/\Delta_{\text{hf}}$; in other words, we treat FWM perturbatively, which is a good approximation in our experiment, except in Figs. 9(c) and 9(d). Furthermore, we approximate [12] $2i\sigma \to i\frac{\omega}{v_g} - \frac{\omega^2}{L\Gamma_E^2}$, where $v_g = \frac{2\Omega^2}{\alpha_0 \gamma}$ is the EIT group velocity and $\Gamma_E = \frac{\Omega^2}{\gamma\sqrt{\alpha_0 L/2}}$ is the width of the EIT transparency window. We then find

$$f_1(z,t') \approx \frac{\Gamma_E e^{-\Gamma_E^2 \frac{L}{4z}(t'-z/v_g)^2}}{2\sqrt{\pi z/L}} \approx \delta(t' - z/v_g), \tag{A11}$$

$$f_2(z,t') \approx \Delta_R^2 \left[-\frac{e^{-\Gamma_E^2 \frac{L}{4z}(t'-z/v_g)^2}}{2\Gamma_E\sqrt{\pi L/z}} + \frac{1}{2}|t'| + \frac{1}{2}t'\text{erf}\left\{ \frac{\Gamma_E(z/v_g - t')}{2\sqrt{z/L}} \right\} \right] \approx \Delta_R^2 t' \Pi[0, z/v_g](t'), \tag{A12}$$

$$f_3(z,t') \approx \frac{i\Delta_R}{2} \left(\text{sgn}[t'] + \text{erf}\left\{ \frac{\Gamma_E(z/v_g - t')}{2\sqrt{z/L}} \right\} \right) \approx i\Delta_R \Pi[0, z/v_g](t'), \tag{A13}$$

$$g_2(z,t') \approx \Delta_R^2 \left[-\frac{z\delta(t')}{\Gamma_E^2 L} + \frac{e^{-\Gamma_E^2 \frac{L}{4z}(t'-z/v_g)^2}}{\Gamma_E\sqrt{\pi L/z}} + \frac{z/v_g - t'}{2} \left(\text{erf}\left\{ \frac{\Gamma_E(z/v_g - t')}{2\sqrt{z/L}} \right\} + \text{sgn}[t'] \right) \right] \approx \Delta_R^2 (z/v_g - t') \Pi[0, z/v_g](t'), \tag{A14}$$

$$g_3(z,t') = -f_3(z,t'). \tag{A15}$$

Here erf is the error function, the sign function $\mathrm{sgn}[t'] = 1$ for $t' \geqslant 0$ and -1 otherwise, and the box function $\Pi[x,y](t) = 1$ for $x < t < y$ and 0 otherwise. The second approximation in Eqs. (A11)–(A15) is done in the limit $\Gamma_{\mathrm{E}} \to \infty$ (the case of an infinitely wide EIT window). Using the $\Gamma_{\mathrm{E}} \to \infty$ expressions, we arrive at Eqs. (6) and (7).

In Figs. 10(a)–10(d), we plot the functions f_j and g_j for $j = 1,2,3$ and the two approximate forms described above. Red curves depict the results of numerical integration of Eqs. (A6)–(A10), with experimental variables $\alpha_0 L = 80$ and $\Omega/(2\pi) = 10$ MHz, so that $\Delta_{\mathrm{R}}/(2\pi) = -14.6$ kHz, $\Gamma_{\mathrm{E}}/(2\pi) = 105$ kHz, and $v_g/(2\pi L) = 16.7$ kHz. Because the light pulses $\mathcal{E}$ and $\mathcal{E}'^*$ have a finite bandwidth, we chose an integration bandwidth of $(2\pi)160$ MHz, and we have checked that a larger range does not significantly affect the results. Solid black curves in Figs. 10(a)–10(d) plot the first approximations in Eqs. (A11)–(A15); dashed black lines show the corresponding $\Gamma_{\mathrm{E}} \to \infty$ expressions in Eqs. (A11)–(A15).

Let us now compute $S(z,t)$. From Eqs. (4) and (5), we have

$$S(z,\omega) = -\frac{g\sqrt{N}\Omega}{F}\left[\mathcal{E}(z,\omega) - i\frac{\Gamma - i\omega}{\Delta_{\mathrm{hf}}}\mathcal{E}'^*(z,\omega)\right], \tag{A16}$$

where $\mathcal{E}(z,\omega)$ and $\mathcal{E}'^*(z,\omega)$ are given in Eq. (A3).

We can then write

$$S(z,t) = \int dt'\mathcal{E}(0,t-t')h_1(z,t') + \int dt'\mathcal{E}(0,t-t')h_2(z,t') + \int dt'\mathcal{E}'^*(0,t-t')h_3(z,t'), \tag{A17}$$

where h_1 describes pure EIT, while h_2 and h_3 are the results of FWM. Functions h_j can be computed as

$$h_1(z,t') = \frac{1}{2\pi}\int d\omega \frac{-g\sqrt{N}\Omega}{F}e^{2i\sigma z}e^{-i\omega t'}, \tag{A18}$$

$$h_1(z,t') + h_2(z,t') = \frac{1}{2\pi}\int d\omega \frac{-g\sqrt{N}\Omega}{F}e^{i\sigma z}\left[\cosh(\xi z) + \left(i\frac{\sigma}{\xi} - \frac{2\Delta_{\mathrm{R}}(\Gamma - i\omega)}{\beta\Delta_{\mathrm{hf}}}\right)\sinh(\xi z)\right]e^{-i\omega t'}, \tag{A19}$$

$$h_3(z,t') = \frac{1}{2\pi}\int d\omega \frac{g\sqrt{N}\Omega}{F}e^{i\sigma z}\left[i\frac{\Gamma - i\omega}{\Delta_{\mathrm{hf}}}\cosh(\xi z) + \left(\frac{\sigma(\Gamma - i\omega)}{\xi\Delta_{\mathrm{hf}}} - i\frac{2\Delta_{\mathrm{R}}}{\beta}\right)\sinh(\xi z)\right]\mathcal{E}^{-i\omega t'}. \tag{A20}$$

Expanding h_2 to $O(1/\Delta_{\mathrm{hf}}^2)$ and h_3 to $O(1/\Delta_{\mathrm{hf}})$, the above expressions simplify to

$$h_2(z,t')$$
$$\approx \frac{1}{2\pi}\int d\omega \frac{g\sqrt{N}\Omega^3[F + e^{2i\sigma z}(2i\Omega^2\sigma z - F)]}{F\Delta_{\mathrm{hf}}^2(\omega + i\Gamma_0)^2}e^{-i\omega t'}, \tag{A21}$$

$$h_3(z,t')$$
$$\approx \frac{1}{2\pi}\int d\omega \frac{g\sqrt{N}\Omega(\Omega^2 e^{2i\sigma z} - F)}{\Delta_{\mathrm{hf}}(\omega + i\Gamma_0)F}e^{-i\omega t'}. \tag{A22}$$

Taking $\delta = \delta_s$, $\gamma_0 = 0$, $2i\sigma \approx i\frac{\omega}{v_g} - \frac{\omega^2}{L\Gamma_{\mathrm{E}}^2}$, and $F \approx \Omega^2$, we have

$$h_j(z,t') \approx -\frac{g\sqrt{N}}{\Omega}f_j(z,t') \tag{A23}$$

for $j = 1,2,3$, where the expressions for $f_j(z,t')$ are given in Eqs. (A11)–(A13). Plugging Eq. (A23) into Eq. (A17) yields an expression that is proportional to the signal field $\mathcal{E}(z,t)$ in Eq. (A4). Thus, under these approximations, we obtain Eq. (16), which is, remarkably, the usual EIT relation. Specifically, in the limit of an infinitely wide EIT window, $S(z,t)$ can be found by plugging Eq. (A23) [with the corresponding $\Gamma_{\mathrm{E}} \to \infty$ expressions for f_j from Eqs. (A11)–(A13)] into Eq. (A17) to yield Eq. (15). The expressions for $|h_1(L,t)|$, $|h_2(L,t)|$, and $|\mathrm{Im}[h_3(L,t)]|$ are plotted in Figs. 10(a'), 10(b'), and 10(c'), respectively. As before, red traces depict the results of numerical integration of Eqs. (A18)–(A20) with the same input parameters as in the f_j and g_j analysis. The solid black curves plot Eq. (A23) using the finite Γ_{E} expressions for f_j from Eqs. (A11)–(A13). The dashed black lines show the corresponding $\Gamma_{\mathrm{E}} \to \infty$ expressions.

[1] M. D. Lukin, Rev. Mod. Phys. **75**, 457 (2003).

[2] H. J. Kimble, Nature (London) **453**, 1023 (2008).

[3] A. I. Lvovsky, B. C. Sanders, and W. Tittel, Nature Photonics **3**, 706 (2009).

[4] K. Hammerer, A. S. Sørensen, and E. S. Polzik, Rev. Mod. Phys. **82**, 1041 (2010).

[5] C. Simon *et al.*, Eur. Phys. J. D **58**, 1 (2010).

[6] M. D. Lukin, M. Fleischhauer, A. S. Zibrov, H. G. Robinson, V. L. Velichansky, L. Hollberg, and M. O. Scully, Phys. Rev. Lett. **79**, 2959 (1997).

[7] H. Kang, G. Hernandez, and Y. Zhu, Phys. Rev. A **70**, 061804 (2004).

[8] V. Wong, R. S. Bennink, A. M. Marino, R. W. Boyd, C. R. Stroud, and F. A. Narducci, Phys. Rev. A **70**, 053811 (2004).

[9] K. I. Harada, T. Kanbashi, M. Mitsunaga, and K. Motomura, Phys. Rev. A **73**, 013807 (2006).

[10] G. S. Agarwal, T. N. Dey, and D. J. Gauthier, Phys. Rev. A **74**, 043805 (2006).

[11] T. Hong, A. V. Gorshkov, D. Patterson, A. S. Zibrov, J. M. Doyle, M. D. Lukin, and M. G. Prentiss, Phys. Rev. A **79**, 013806 (2009).

[12] N. B. Phillips, A. V. Gorshkov, and I. Novikova, J. Mod. Opt. **56**, 1916 (2009).

[13] M. Fleischhauer, A. Imamoglu, and J. P. Marangos, Rev. Mod. Phys. **77**, 633 (2005).

[14] M. Fleischhauer and M. D. Lukin, Phys. Rev. Lett. **84**, 5094 (2000); Phys. Rev. A **65**, 022314 (2002).

[15] A. V. Gorshkov, A. André, M. Fleischhauer, A. S. Sørensen, and M. D. Lukin, Phys. Rev. Lett. **98**, 123601 (2007).

[16] I. Novikova, A. V. Gorshkov, D. F. Phillips, A. S. Sørensen, M. D. Lukin, and R. L. Walsworth, Phys. Rev. Lett. **98**, 243602 (2007).

[17] N. B. Phillips, A. V. Gorshkov, and I. Novikova, Phys. Rev. A **78**, 023801 (2008).

[18] A. V. Gorshkov, A. André, M. D. Lukin, and A. S. Sørensen, Phys. Rev. A **76**, 033805 (2007).

[19] E. E. Mikhailov, Y. Rostovtsev, and G. Welch, J. Mod. Opt. **49**, 2535 (2002); **50**, 2645 (2003).

[20] R. M. Camacho, P. K. Vudyasetu, and J. C. Howell, Nature Photonics **3**, 103 (2009).

[21] As in Refs. [14, 15, 18], we define the Rabi frequency Ω as $\Omega^2 = \wp_{es}^2 I/(2\hbar^2\epsilon_0 c)$, where I is the control intensity.

[22] M. D. Rotondaro and G. P. Perram, Phys. Rev. A **58**, 2023 (1998).

[23] M. D. Lukin, A. B. Matsko, M. Fleischhauer, and M. O. Scully, Phys. Rev. Lett. **82**, 1847 (1999).

[24] E. Cerboneschi and E. Arimondo, Phys. Rev. A **54**, 5400 (1996).

[25] M. D. Lukin, P. R. Hemmer, M. M. Löffler, and M. O. Scully, Phys. Rev. Lett. **81**, 2675 (1998).

[26] A. Raczyński and J. Zaremba, Opt. Commun. **209**, 149 (2002).

[27] A. Raczyński, J. Zaremba, and S. Zielińska-Kaniasty, Phys. Rev. A **69**, 043801 (2004).

[28] F. E. Zimmer, A. André, M. D. Lukin, and M. Fleischhauer, Opt. Commun. **264**, 441 (2006).

[29] A. Eilam, A. D. Wilson-Gordon, and H. Friedmann, Opt. Lett. **33**, 1605 (2008).

[30] P. Kolchin, S. Du, C. Belthangady, G. Y. Yin, and S. E. Harris, Phys. Rev. Lett. **97**, 113602 (2006).

[31] P. Kolchin, Phys. Rev. A **75**, 033814 (2007).

[32] P. Kolchin, C. Belthangady, S. Du, G. Y. Yin, and S. E. Harris, Phys. Rev. Lett. **101**, 103601 (2008).

[33] K. Drese and M. Holthaus, Eur. Phys. J. D **5**, 119134 (1999).